Groundwater
Monitoring&Remediation

Diagnostic Tools to Assess Mass Removal Processes During Pulsed Air Sparging of a Petroleum Hydrocarbon Source Zone

by Daniel Bouchard, Massimo Marchesi, Eugene L. Madsen, Christopher M. DeRito, Neil R. Thomson, Ramon Aravena, Jim F. Barker, Tim Buscheck, Ravi Kolhatkar, Eric J. Daniels, and Daniel Hunkeler

Abstract

During remediation of contaminated aquifers, diagnostic tools can help evaluate whether an intended mass removal process was successfully initiated and acted on specific contaminants of concern. In this study, several diagnostic tools were tested in a controlled-release in situ air sparging experiment that focused on the treatment of target hydrocarbons (e.g., benzene, toluene, ethylbenzene, and xylenes). The tools included compound-specific isotope analysis (CSIA), expression of functional genes (mRNA), and metabolites characteristic of aerobic and anaerobic biodegradation. Total and compound-specific mass balances were established and used, along with traditional monitoring parameters, to validate the results from the various tools. CSIA results indicated biodegradation as the main process contributing to benzene and toluene removal. Removal process-specific isotope shifts were detected in groundwater as well as in the system effluent gas. CSIA, metabolite, and mRNA biomarkers consistently indicated that both aerobic and anaerobic biodegradation of benzene and toluene occurred, but that their relative importance evolved over time and were related to the treatment system operation. While the indicators do not allow quantification of the mass removed, they are particularly useful to identify if a removal process has been initiated, and to track relative changes in the predominance of in situ contaminant attenuation processes resulting from remediation efforts.

Introduction

In situ remediation methods aim to promote physical, chemical, and/or biological contaminant removal processes (Suthersan and Payne 2004; NAVFAC 2005; Krembs et al. 2010). In complex systems, it is often difficult to assess and quantify the relative contributions of simultaneously occurring mass removal processes (Madsen 1991; Bomback et al. 2010). For instance, during in situ air sparging (IAS) at petroleum hydrocarbon (PHC) contaminated sites, the assessment of biodegradation can be challenging because physical removal by volatilization may also occur and can be indistinguishable based on concentration data alone. The volatilization rate depends on a number of factors such as the distribution and density of the air channel network (Tomlinson et al. 2003), geological heterogeneities (Hall et al. 2000), the air injection mode and flow rate (Rogers and Ong 2000), and the nonaqueous phase liquid (NAPL) entrapment architecture (Waduge et al. 2004). Several approaches have been proposed to evaluate the efficiency of an IAS system to promote volatilization such as: monitoring the spatial and temporal concentration changes of volatile organic compounds (VOCs); using dissolved oxygen (DO) in groundwater as an indicator of air contact; observing water and soil gas pressures around injection points (Bass et al. 2000; Hall et al. 2000; Johnson et al. 2001b); and performing tracer tests (Bruce et al. 2001; Johnson et al. 2001a; Berkey et al. 2003). While these approaches evaluate volatilization or oxygen delivery, they do not demonstrate whether biodegradation of specific compounds is occurring. Assessing treatment performance based on DO concentrations can be unclear and misleading, as low DO concentrations can be due to poor air distribution (Johnson et al. 1997; Johnston et al. 1998) or consumption during aerobic biodegradation (Kao et al. 2008). A mass balance approach relying on VOC and CO_2 fluxes may be suitable to assess the overall contaminant mass that has volatilized or biodegraded (Aelion and Kirtland 2000); however, the relative importance of the removal processes for specific contaminants of concern, such as benzene, are not determinable from such data. Understanding the predominant mass removal mechanism(s) responsible for reducing the concentration of contaminants of concern can

Article impact statement: Diagnostic tools (CSIA, metabolites, functional genes) provide compound- and process-specific insight into contaminant removal processes during in situ air sparging.

doi: 10.1111/gwmr.12297

be used to help optimize the cost-effectiveness of remediation efforts. While physical contaminant removal of target compounds can usually be assessed based on the extracted mass in the off-gas, there is a need for tools to demonstrate biodegradation of specific compounds during IAS.

There are several possible tools that can potentially provide compound- and process-specific information about contaminant removal processes during IAS. The compound-specific isotope analysis (CSIA) method consists of tracking the progressive shifts of carbon ($\delta^{13}C$) and hydrogen ($\delta^{2}H$) isotope ratios for a given VOC. Molecules with light isotopes are degraded faster and thus, the heavy isotopes become increasingly enriched in the remaining contaminant mass. The magnitude of the isotope ratio shift depends on the isotope enrichment factor associated with specific processes. Under oxic and anoxic conditions, hydrocarbons are degraded by distinct mechanisms, hence different patterns of isotope fractionation (for both $\delta^{13}C$ and $\delta^{2}H$) can be observed (Elsner et al. 2005; Zwank et al. 2005). Physical removal processes can also cause characteristic isotopic shifts although these shifts typically tend to be smaller (Buscheck et al. 2009; Kuder et al. 2009). Thus, the effect of physical processes on isotope ratios may only become apparent after a large fraction of compound has been removed. Previous studies have reported $\delta^{13}C$ and $\delta^{2}H$ isotope fractionation patterns for various VOCs during air-water partitioning (Slater et al. 1999; Kuder et al. 2009) and air-NAPL equilibration (Harrington et al. 1999; Hunkeler et al. 2001b; Wang and Huang 2003; Aelion et al. 2010), which were distinctly different from those for biodegradation. Therefore, the magnitude and direction of $\delta^{13}C$ and $\delta^{2}H$ isotope shifts may serve as criteria for distinguishing between physical removal processes and aerobic or anaerobic biodegradation. This information can potentially reveal the relative contribution or predominance of different mass removal processes occurring in situ under natural conditions or induced by active treatment efforts.

In parallel with CSIA, specific biomarkers (metabolites and expressed biodegradation genes) have been identified that are diagnostic of biodegradation at contaminated sites (Bomback et al. 2010; Jeon and Madsen 2013). These include a limited array of genes that encode enzymes involved in the biodegradation of diverse PHCs (Madsen 2000). The expression of biodegradation genes, for example, transcription of DNA into messenger RNA (mRNA), indicates that the metabolic process of biodegradation has been activated. Consequently, detection of mRNA transcripts provides much stronger evidence for biodegradation processes than DNA-based assays (Nebe et al. 2009; Abu Laban et al. 2010; Busi da Silva and Corseuil 2012). In addition, active in situ metabolism of compounds by naturally occurring microbial populations lead to the formation of compound-specific metabolites uniquely formed during the biodegradation process. Therefore, the presence of specific metabolites in groundwater confirms in situ enzymatic attack of the related primary compound (Beller et al. 1995; Wilson and Madsen 1996; Martienssen et al. 2006; Martus and Schaal 2010). The specificity of selected mRNAs and metabolites make biomarker analysis an attractive diagnostic tool that, combined with CSIA, can provide additional information to improve remediation performance assessment. Such a combined approach has previously been applied to document natural attenuation (Griebler et al. 2004; Beller et al. 2008; Morasch et al. 2011) but not yet in the context of an IAS application.

The objective of this study was to evaluate the utility of CSIA and biomarkers (both biodegradation genes and metabolites) to provide compound and process-specific insight into mass removal processes during the IAS treatment of a PHC source zone. In particular, we evaluated whether these diagnostic tools could be used to demonstrate biodegradation of specific compounds in addition to physical removal. The study was performed under highly controlled conditions where an IAS system combined with a vapor extraction system was operated for approximately 400 days to treat an emplaced synthetic PHC mixture. This approach has the advantage that the diagnostic tool response can be corroborated with removal rates obtained from a mass balance of the total PHC mixture or individual compounds. The application of the diagnostic tools in this study focused on benzene and toluene, which are often the main contaminants of concern at PHC sites. In addition to CSIA and biomarkers, conventional data (e.g., DO, dissolved VOC concentrations, geochemistry, and effluent gas O_2 and CO_2 concentrations) were collected for comparison. For CSIA, in addition to groundwater samples which reflect processes at a smaller scale, gas samples were analyzed to evaluate whether removal processes, especially biodegradation, can also be identified based on the isotope signature in the effluent gas, which integrates a response from the entire treatment zone.

Materials and Methods

Field Site

This study was performed in the experimental cell (Figure 1) previously used by Nelson et al. (2009) in the sandpit area of the University of Waterloo Groundwater Research Facility at the Canadian Forces Base (CFB) in Borden, ON, Canada. The aquifer at this location consists of well-sorted fine to medium grained sand (Mackay et al. 1986). Although relatively homogenous, stratigraphic layering is evident with sediment sizes ranging from silt to coarse sand thus creating lithologic facies with distinctive hydraulic conductivities (Sudicky 1986; Weissmann et al. 2015). A 4.5 m x 4.5 m area was delimited using Waterloo Barrier® sealable-joint steel sheet-piling driven approximately 7 m below ground surface (bgs) into the underlying aquitard (silty clay unit) thereby hydraulically isolating an undisturbed segment of the aquifer from the natural groundwater flow. Two stainless steel air sparging points (3 cm inside diameter, ID) were driven to a depth of 4.4 m bgs (Figure 1) and connected to an air compressor (DeWalt). Each sparging point consisted of a cylindrical stainless steel housing (20 cm in length and 3 cm in diameter) with a ring of four 0.8-cm-diameter holes spaced every 2.5 cm along the length and covered with a stainless steel screen. A coarse gravel-sized crushed stone was used to fill the cell from ground surface to the top of the sheet-piling that extended approximately 30 cm above ground surface. A wooden cap covered with a

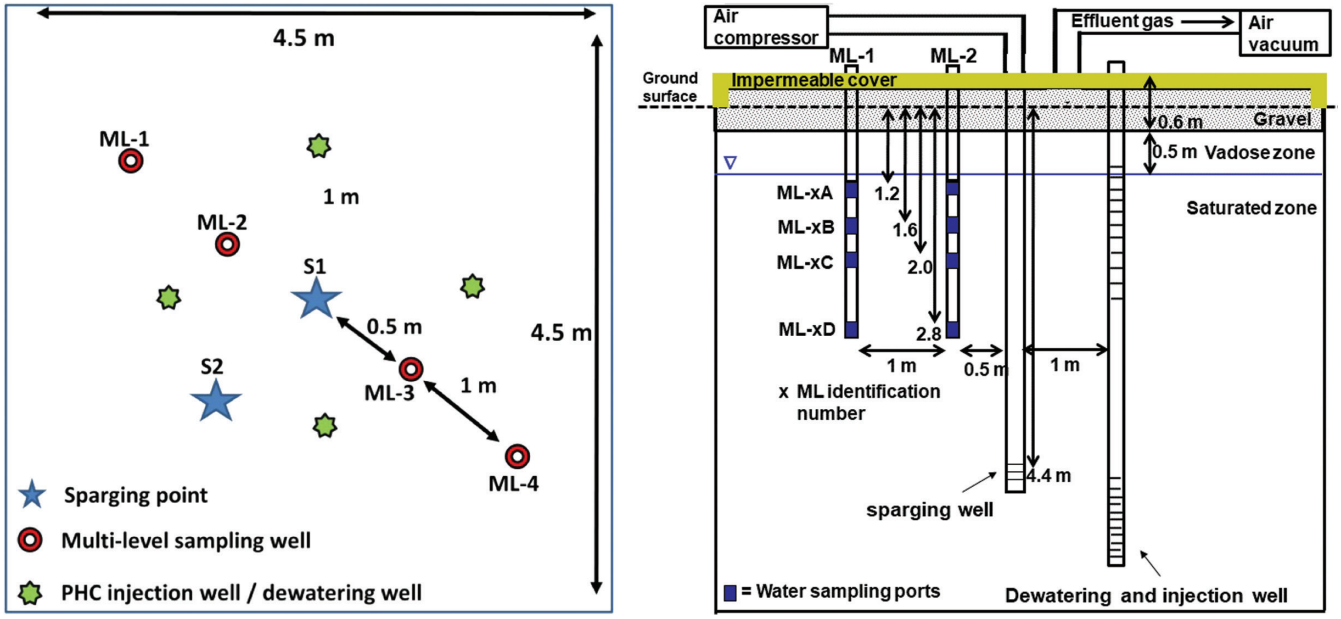

Figure 1. Plan (left) and cross-sectional (right) view of the experimental cell in which a 152 L petroleum hydrocarbon source was injected. The plan view presents the location of the monitoring wells and air injection points. The cross-sectional view shows the air-sparging and vapor extraction systems, sampling wells (ML) with ports at four sampling depths (ML-A, -B, -C, and -D). Note that monitoring wells ML-3 and ML-4 (positioned on the right side of the sparging point) are not shown on the cross-sectional view for simplicity.

Table 1

Source Composition and Selected Physico-Chemical Properties from Yaws (1999)

Compound	Volume (L)	MW (g)	Mole Fraction (%)	Henry's Law Constant (air/water)	Water Solubility (mg/L)	Vapor Pressure (mm Hg)
Isopentane	50	72	36.0	55.8	47.8	696.2
Cyclopentane	20	70	18.1	7.7	156	313.8
Octane	20	114	10.4	199.9	0.66	7.8
2,2,4-Trimethylpentane	50	114	25.6	141.0	2.44	49.0
Benzene	5	78	4.7	0.224	1755	96.5
Toluene	2.5	92	2.0	0.260	542.4	28.3
o-Xylene	1	106	0.7	0.171	220.8	6.6
1-2-4 Trimethylbenzene	1	120	0.6	0.277	52.66	2.2
Naphthalene	2	128	1.5	0.017	32.05	0.3
MTBE	0.5	88	0.4	0.022	51,260	248.5

Note: MTBE, methyl tert-butyl ether.

synthetic geomembrane was built over the cell to minimize air leakage. A PVC pipe (5.1 cm ID) was installed in the middle of the cap and served as the location where the effluent gas was extracted. For groundwater sampling, four multilevel (ML) piezometers each comprised of four 5-cm long sampling points were installed along a diagonal transect across the cell (Figure 1). The sampling points were located at 1.2, 1.6, 2.0 and 2.8 m bgs, and denoted as ML-xA, ML-xB, ML-xC, and ML-xD, respectively (*x* is the ML identification number).

PHC Source Composition and Source Injection

A synthetic gasoline source was prepared using four alkanes, four monoaromatic hydrocarbons, one polyaromatic hydrocarbon, and one fuel oxygenate (Fluka, grade >95%) (Table 1). The total NAPL volume was 152 L (105.2 kg), and the mole fraction of each compound varied between 0.4 and 36%. The previous experiment conducted in the cell (Nelson et al. 2009) involved the injection of light alkanes (pentane, hexane, isohexane, and methylcyclopentane) added to a soltrol mixture (mixture of decane, undecane, dodecane, and tridecane). The remaining light alkanes and soltrol mass within the cell was estimated to be 37 and 25 kg, respectively. Fourteen days before the IAS system was started, the new synthetic PHC mixture was introduced into the cell using four injection wells under gravity-driven conditions (Figure 1). Each injection well was double screened, with the lower

screened interval used to draw the water table down and the upper screened interval used for NAPL injection. Following injection, the water table was lowered several times over a 4-day period by pumping followed by recovery to generate a NAPL smear zone. An oil-water interface probe (Solinst, California) was used to measure the NAPL thickness in each injection well.

IAS System Operation

The treatment system was operational for 284 days (Day 1 to 60, and Day 157 to 380), and was shut down for 96 days (from Day 61 to Day 156) due to winter conditions (denoted as winter recess). The sparging point located in the middle of the cell (S1; Figure 1) was used from Day 1 to Day 270 (except for the winter recess), and the sparging point (S2) was used toward the end of the experiment (Day 270 to Day 380) to maximize VOC mass removal. The system was operated in pulsed mode consisting of 1 h of air injection (targeted air flow rate of 125 L/min) followed by a 1-h shut-off (no flow). The flow rate used for the vapor extraction system corresponded to the injection air flow rate.

Sampling and Analyses

Baseline groundwater sampling was performed in two phases. Phase 1 was conducted 42 days before source injection and focused on biomarkers (metabolites and mRNA). Phase 2 was performed 10 days after source injection to characterize the hydrochemical conditions and stable isotope composition of the VOCs and dissolved inorganic carbon (DIC). The results from those two phases constitute the baseline data and are shown at Day 0 on figures for simplicity. During IAS system operation, the frequency of groundwater sampling varied for each parameter. More frequent sampling (days to weeks) was conducted during the first few weeks of system operation, followed by less frequent sampling (monthly to bimonthly) at later times.

Groundwater was extracted using a peristaltic pump (Masterflex) and samples were collected for analysis after stabilization of field parameters (pH, DO, temperature, electrical conductivity, and ORP). Groundwater samples for the analysis of NO_3^-, SO_4^{2-}, and dissolved Fe^{2+} were collected in 20-mL HDPE bottles. Samples for dissolved Fe^{2+} analysis were preserved with HCl. Groundwater samples for the quantification of VOCs, CSIA ($\delta^{13}C$ and $\delta^{2}H$) of VOCs, DIC, $\delta^{13}C$ of DIC, and methane were collected in 40-mL VOC glass vials with Teflon-lined silicone septa containing NaN_3 (1%) to inhibit microbial activity. $^{13}C/^{12}C$ and $^{2}H/^{1}H$ ratios are expressed using the δ notation ($\delta^{13}C$ and $\delta^{2}H$) relative to the international reference standard as given by.

$$\delta\left[{}^{0}/_{00}\right] = \left(R/R_{std} - 1\right) * 1000 \quad (1)$$

where R and R_{std} are the isotope ratio of the sample and the international reference standard, Vienna Pee Dee Belemnite (VPDB) for carbon and Vienna Standard Mean Ocean Water (VSMOW) for hydrogen, respectively. The average standard deviation for benzene and toluene was 0.2‰ for carbon and 5‰ for hydrogen (n = 10 for each compound). The analytical methods are described in the Appendix S1, Supporting Information.

For metabolites, two 1-L glass bottles were filled with groundwater. One of them was stabilized with HCl (pH < 2) and the other with NaOH (pH > 8). The samples were shipped on ice and refrigerated until analysis by GC/MS. For diagnostic purposes, the most informative biomarker metabolites are those whose molecular structure strongly resembles that of the parent contaminant; these occur early in the metabolic pathways. In this work, we analyzed three compound-specific metabolites that are uniquely of microbial origin: (1) benzene *cis*-dihydrodiol (bz-diol), indicative of aerobic benzene degradation (Wilson and Madsen 1996; Diaz et al. 2013); (2) toluene *cis*-dihydrodiol (to-diol), indicative of aerobic toluene degradation (Wilson and Madsen 1996; Diaz et al. 2013); and (3) benzylsuccinate, indicative of anaerobic toluene degradation (Beller et al. 2008; Fuchs et al. 2011). In addition *o*-cresol was quantified, which is strongly associated with aerobic toluene biodegradation (Whited and Gibson 1991; Diaz et al. 2013).

For mRNA assays, 1L groundwater was extracted and filtered through Sterivex filters (0.2 μm). After being purged with air, the Sterivex filters were then frozen immediately on dry ice and maintained at −80 °C until mRNA was extracted and analyzed using reverse transcriptase quantitative PCR (RTqPCR). We analyzed mRNA of: (1) toluene dioxygenase (todC), associated with biodegradation of three aromatic compounds (benzene, toluene, and ethylbenzene) under aerobic conditions (Hendrickx et al. 2006; Cébron et al. 2008; Nebe et al. 2009; Liu et al. 2012); (2) bssA of sulfate reducing bacteria (bssA-SRB), a specific variant of the *bssA* gene associated with anaerobic toluene metabolism under sulfate-reducing conditions (Beller et al. 2008); and (3) anaerobic benzene carboxylase (abcA), characteristic of benzene biodegradation under iron-reducing and other anaerobic conditions (Abu Laban et al. 2010). Details of the analytical methods for metabolites and mRNA extraction are provided in the Appendix S1.

A qualitative assessment of the NAPL distribution in the soil was conducted with an ultraviolet optical screening tool (UVOST, Dakota Technologies, Fargo, North Dakota) 7 days before the IAS system was started (Day −7) and conducted again at the end of the experiment (Day 381). During the final assessment, a soil core was retrieved at location B near ML-1 and ML-2 (Appendix S3, Figure S5). From the core, 13 subsamples were collected at 20 cm intervals from 0.5 to 2.9 m bgs, and were analyzed for bulk VOC concentration. The samples were preserved in glass containers and kept at 4 °C during transport and storage.

For effluent gas sampling, a sampling port was installed between the cell and the vacuum system. During the first 3 weeks of system operation, the sampling frequency was high (0.5 to 2 days), and then was reduced (5 to 7 days). A photoionization detector (PID, MiniRae 2000, RAE Systems, San Jose, California) and an infrared monitor (IRM, Eagle 2, RKI Instruments, Union City, California) were permanently installed to continuously record total VOC and O_2/CO_2, respectively. Gas phase samples were collected in 20-mL glass vials as described in Nelson et al. (2009) for VOC analysis. VOC sampling for CSIA was performed by pumping the effluent gas stream (500 mL/min) through 30 mL of methanol contained in a 40-mL glass vial for 20 min (Bouchard and Hunkeler 2014; Bouchard et al. 2015). Gas samples for CO_2 and ^{13}C in CO_2 were taken with 60-mL syringes and 10-mL vacutainer tubes, respectively.

Mass Balance Estimates

Bulk Mass Balance

To establish a VOC mass balance, the mass removed physically (VOC recovered from the extracted gas phase) and the mass biodegraded (recovered as CO_2 in the extracted gas phase) were independently determined (see Aelion and Kirtland 2000 and the Appendix S2), and then compared to the initial VOC mass (Table 1). The volatilized mass was estimated using the continuous PID data of the effluent gas, which were transformed into total VOC concentration based on the correlation between PID readings and total VOC concentrations from analysis of gas samples as shown in the Figure S1 of Appendix S2. The biodegraded mass was estimated using the temporal CO_2 data assuming that the following stoichiometry for hexane was representative:

$$C_6H_{14} + 9.5O_2 \rightarrow 6CO_2 + 7H_2O \quad (2)$$

Compound-Specific Mass Balance

Since the diagnostic tools provide compound-specific information, mass balances for specific compounds were established for comparison. The temporal evolution of the concentration of each compound was quantified based on the continuous PID data and the time-discrete VOC concentrations, which included all VOCs present in the system. Based on the VOC concentrations and the PID intensity conversion factor provided by the instrument manufacturer (RaeSystems 2016), the PID signal was proportionally attributed to each compound. The VOC proportions were determined for 24 sampling events and estimated by linear interpolation for the time period between sampling events. A time-varying compound extraction rate was obtained by multiplying the concentrations with the extraction system flow rate. The cumulative mass removed for each compound was then quantified by integrating this rate over the entire period that the IAS system operated (284 days).

At the end of the experimental period, the mass physically removed was subtracted from the initial mass injected to estimate the potential mass biodegraded. Since the mass remaining in the cell at the termination of the experiment was not thoroughly evaluated, these estimated values are considered approximate. For compounds present at concentrations below 5 mg/kg in the posttreatment soil core, it is reasonable to assume that the mass not accounted for by volatilization was biodegraded. For compounds detected at higher concentrations in the posttreatment soil core (>5 mg/kg), the mass not accounted for by volatilization provides an upper bound for the biodegraded mass. For VOCs present from the previous experiment (i.e., pentane, hexane, iso-hexane, 3-methylpentane) no assessment was performed due to the uncertain initial mass in the experimental cell.

Results and Discussion

Concentration Data

Concentration data are presented for the first 250 days after starting the IAS system including the winter recess period from Day 61 to 156. Although the IAS system operated until Day 380, concentrations were generally too low to acquire complete diagnostic tool data sets beyond Day 250.

VOCs

At the start of system operation, NAPL with an average thickness of 2.5 ± 0.8 cm was detected in the four injection wells at a depth of 0.96 to 1.01 m bgs, which is consistent with the initial UVOST investigation performed on Day –7. The latter investigation indicated that most of the NAPL was in the upper part of the aquifer (Figure S4 in Appendix S3).

On the day before system start-up (Day 0), the dissolved BTX concentration (sum of benzene, toluene, and xylenes) ranged from 4000 to 10,000 ug/L (Figure 2) in the upper 0.6 m of the aquifer as observed at the upper sampling port of the four ML wells. By Day 21, BTX concentrations were present in the groundwater laterally across the cell and vertically down to approximately 1.2 m below the water table because of the mixing induced by the pulsed IAS system. Between Day 21 and Day 44, BTX concentrations reached their maximum values, with concentrations up to 65,000 ug/L (ML-3A). Beyond Day 44, BTX concentrations decreased and were below method detection limits (MDLs) (2 to 5 µg/L depending on the compound) by Day 214 or Day 248 at half of the sampling locations. The concentrations of other compounds were also low or below MDLs by Day 248 (Table S5 in Appendix S5). The final UVOST assessment (Day 381) indicated absence of NAPL (Figure S4 in Appendix S3). The concentrations in subsamples taken along the length of the soil core (Table S6 in Appendix S5) were below 5 mg/kg (detection limit 0.005 mg/kg), except for isooctane (up to 142 mg/kg), octane (up to 56 mg/kg) and iso-pentane (up to 56 mg/kg).

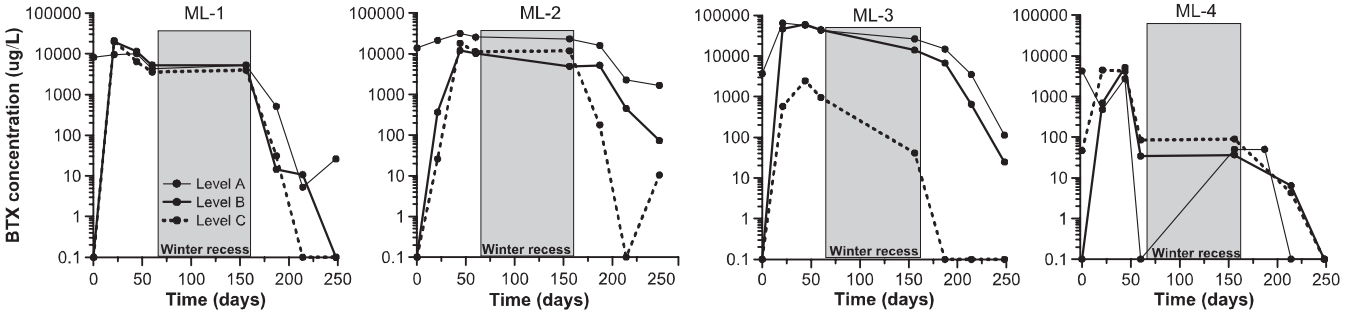

Figure 2. Changes in BTX concentrations over the first 250 days at four monitoring wells (ML-1, ML-2 ML-3, and ML-4) sampled at three sampling depths (levels A, B, and C). The IAS system was not operational from Day 60 to Day 156 (winter recess).

Dissolved Oxygen

The baseline DO concentrations ranged between 4.8 and 6.7 mg/L, except at two locations with lower values (Figure 3A). The average DO concentration (5.3 mg/L) was close to the background value of 4.9 mg/L measured in a well located approximately 2 m outside the cell. In addition, dissolved Fe^{2+} (Figure 3C) and methane (Figure 3E) were detected, and negative ORP values were observed (Figure 3B, average of −107 mV). Before system startup, the experimental cell was likely under anoxic conditions due to the presence of PHC from the previous experiment. Shortly before the baseline sampling event, DO was probably introduced by the induced water table fluctuations. This explains why elevated DO concentrations as well as indicators of anoxic conditions were simultaneously present. Following IAS startup, most sampling locations initially showed a decrease in DO concentration (Day 21), followed by a general increase in DO with strong spatial variation (Day 44 and 60) until the winter recess. However, the DO concentrations remained below the estimated saturation level (10.5 to 12 mg/L O_2 at 7 to 13 °C) consistent with findings from other IAS studies (Johnson et al. 1997; Aelion and Kirtland 2000). The observed spatial and temporal variation in DO concentrations indicates either a strong DO consumption due to a high level of microbial activity, or limited O_2 delivery due to small-scale lower permeability zones that are circumvented (Tomlinson et al. 2003). All monitoring locations were expected to be within the 2.5 m radius of influence observed by Tomlinson et al. (2003) in the Borden aquifer for a relatively equivalent injection depth and air flow rate.

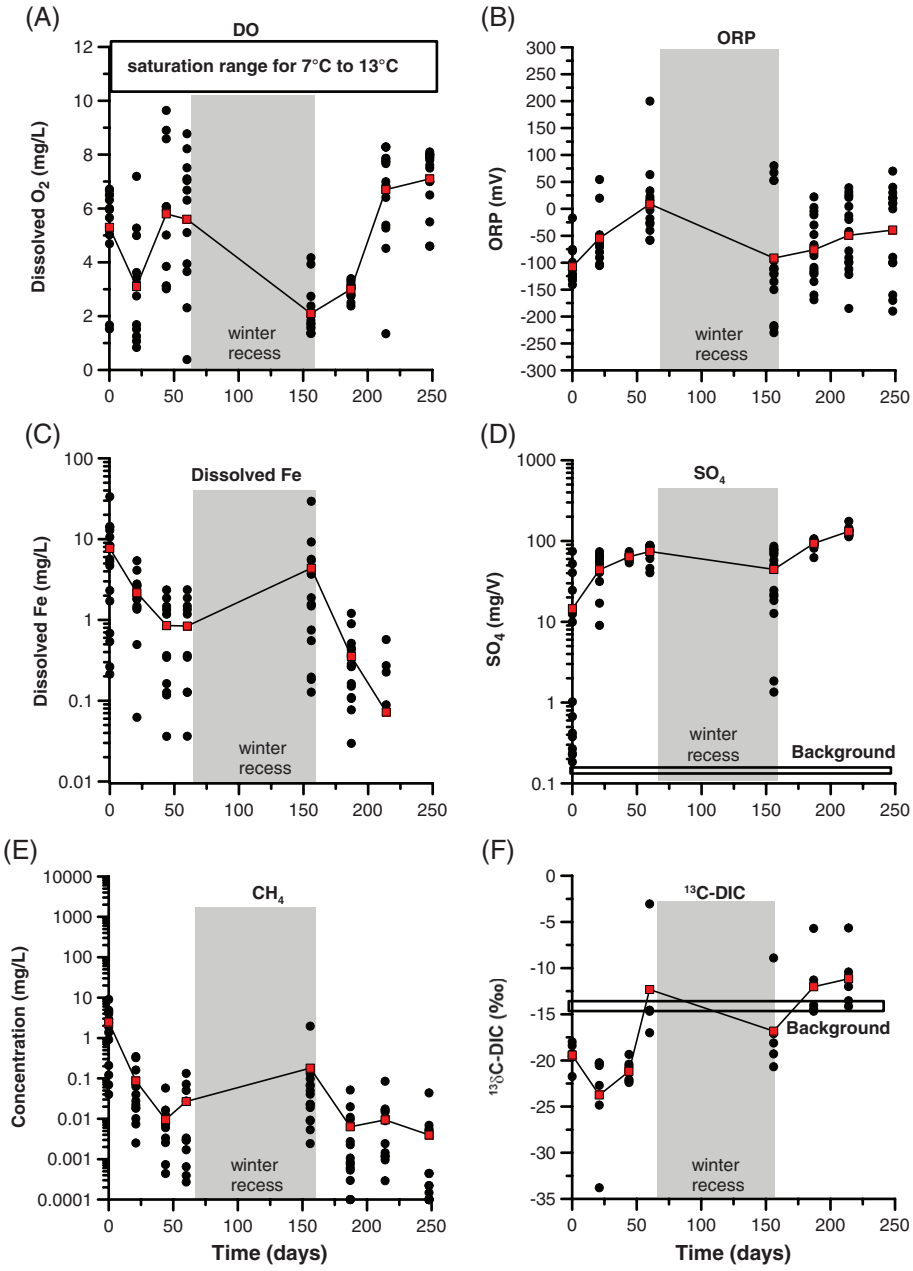

Figure 3. O_2 (A), oxidation reduction potential (ORP) (B), Fe^{2+} (C), SO_4^{2-}(D), and CH_4 (E) at 12 locations (ML-1, 2, 3, and 4), and ^{13}C-DIC (F) at five locations (ML-2A, B and C; ML-3A and C) in the upper 1.0 m of the aquifer. Red square symbols represent average values. The IAS system was not operational from Day 60 to Day 156 (winter recess).

At the end of the winter recess (Day 156), low DO concentrations (average of 2.1 mg/L) were observed (Figure 3A) and ORP values where generally lower (Figure 3B) both indicating a shift to more reducing conditions. The decrease of the average sulfate concentration and the increasing presence of dissolved Fe and methane confirmed the intensification of anoxic conditions. Following restart of the system, the DO concentrations progressively increased and averaged 3.0, 6.7 and 7.1 mg/L at Day 187, 214 and 248, respectively, but remained below saturation levels. These higher DO levels likely reflect that less DO was being consumed by biodegradation of the increasingly scarce hydrocarbons. Finally, ORP values remained negative at several sampling points at Day 214 and 248 (average of −49.1 and −39.3 mV, respectively). The DO, dissolved iron, dissolved methane, and ORP results indicate the coexistence of oxic and anoxic conditions throughout IAS operation.

$\delta^{13}C$ in DIC

Results for $\delta^{13}C$ in the DIC ($\delta^{13}C$-DIC) at ML-2 (Level A, B, and C) and ML-3 (Level A and C) are shown in Figure 3F. The DIC became depleted in ^{13}C between Day 1 and 21, and then more enriched again on Day 60. During winter recess, the DIC again became more depleted in ^{13}C followed by enrichment during the subsequent treatment phase (Figure 3F). These shifts likely reflect the interplay between two processes, production of CO_2 by biodegradation and removal of CO_2 by sparging. The former leads to a shift of the $\delta^{13}C$ to more negative values as the PHCs from which the CO_2 is produced are depleted in ^{13}C (average $\delta^{13}C$ of −27.2‰) relative to the background DIC. The latter leads to a shift in the opposite direction due to the removal of CO_2 depleted in ^{13}C. Over the initial 21 days, CO_2 production was probably the largest due to the high availability of VOCs and then slowed down. This is consistent with DO concentrations, which were generally lowest on Day 21 (Figure 3A). Thus after an initial shift to more negative $\delta^{13}C$ values due to intense CO_2 production, the effect of the IAS operation shifted the values in the positive direction. During winter recess, the shift in the negative direction was due to production of CO_2, which was followed by an increasing trend once the IAS system was restarted on Day 157. After winter recess, the $\delta^{13}C$ values were generally more positive than before the winter recess. Biodegradation was likely less intense due to the lower VOC availability at later time. Methanogenesis likely had only minor influence since it would cause a shift in the $\delta^{13}C$ of DIC in the opposite direction (Landmeyer et al. 1996; Whiticar 1999) during winter recess than what was observed.

Gaseous O_2 and CO_2

Short-term changes in O_2 and CO_2 concentrations in the effluent gas during air sparging pulses (60 min) are illustrated in the Appendix S6 for three 400-min periods before and after winter recess (Figure S7 in Appendix S6). During the first two periods (Day 2 and Day 21), large O_2 and CO_2 fluctuations that are synchronized with the 1-h on-off pulsed IAS system operation are observed. O_2 concentrations increased during air injection while CO_2 concentrations dropped. For the subsequent four sampling periods, the fluctuation in O_2 and CO_2 concentrations gradually diminished (Day 44, Day 156) until no change was observed by Day 187 and Day 214. This decrease in the amplitude of O_2 and CO_2 fluctuations reflects a decrease in biodegradation activity consistent with the change in ^{13}C-DIC values (Figure 3F) and increase in DO concentration (Figure 3A).

VOC Mass Balance

Bulk Mass Balance

The total VOC mass removed by the combination of volatilization and biodegradation was estimated to be 92% ± 20% (Figure 4). During the prewinter treatment period (from Day 1 to Day 60) volatilization was the dominant mass removal mechanism but the contribution of biodegradation to the total mass removed increased from 18% on Day 10 to 25% on Day 60. During the postwinter treatment period (from Day 156 to Day 380) volatilization remained the dominant removal process. Over the entire treatment period, 70% of the mass was removed by volatilization and 30% by biodegradation. A predominance of volatilization over biodegradation has also been reported in other IAS studies (Johnston et al. 1998; Aelion and Kirtland 2000).

Compound-Specific Mass Balance

The controlled experimental setting provided the opportunity to establish compound-specific mass balances (Table 2), which allows assessing the dominant mass removal process (volatilization or biodegradation) on a compound basis. These mass balances also serve as a reference to further validate the compound-specific diagnostic tool results. The alkanes (isopentane, cyclopentane and isooctane) were mainly physically removed (through volatilization), except for octane (mainly biodegraded). In contrast, biodegradation was the dominant removal mechanism for the aromatic

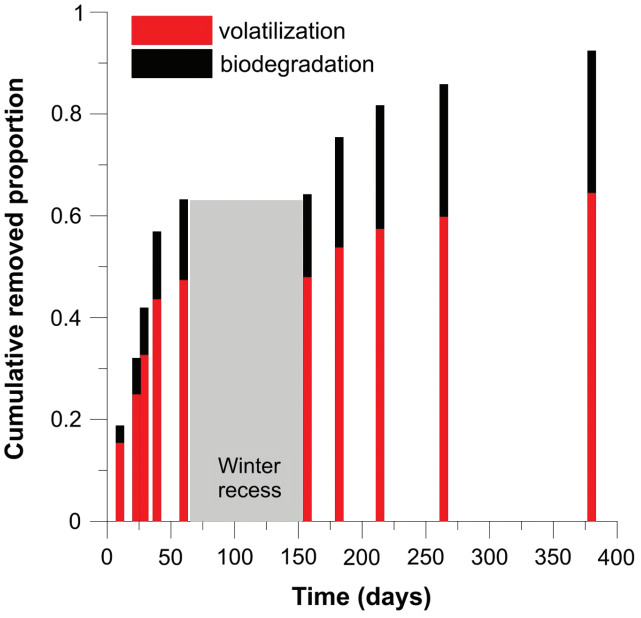

Figure 4. Relative contribution of volatilization and biodegradation to VOC removal. The IAS system was not operational from Day 60 to Day 156 (winter recess).

Table 2

Compound-Specific Mass Balance Calculated for Six VOCs Exiting the Experimental Cell (Effluent Gas) Using PID Data Adjusted with Time-Discrete Concentration Data Determining by GC/PID

	Initial Mass Injected	Mass Volatilized	Removal Process Contribution	
			Volatilization	Biodegradation
Compound	g	g	%	%
Isopentane	30,800	17,000	55	≤45
Cyclopentane	15,020	8000	53	47
Isooctane	34,600	24,000	69	≤31
Octane	14,050	2100	15	≤85
Benzene	4383	800	18	82
Toluene	2167	500	23	77
o-Xylene	864	300	35	65

Notes: PID, photoionization detector; VOC, volatile organic compound. The mass biodegraded was estimated based on the difference between the total and the volatilized mass. For compounds that were present at concentrations >5 mg/kg in a soil core at the end of the experiment, the estimated mass biodegraded provides an upper limit (see text for details). The uncertainty of the volatilized mass is ±20%.

compounds (BTX). A relationship between the dominant removal process and water solubility (Table 1) of the compounds can be observed. Compounds with higher water solubility (i.e., monoaromatic compounds) were predominantly biodegraded, likely due to their increased availability to active microbial populations carrying out biodegradation. Numerical modeling of BTEX removal during IAS has also suggested preferential biodegradation compared to volatilization for one of the two field sites investigated by Rahbeh and Mohtar (2007).

Diagnostic Tools

Compound-Specific Isotope Analysis

Groundwater: CSIA data were evaluated using dual carbon and hydrogen isotope plots. On these plots, changes in the isotope ratio relative to the original source signatures are plotted and compared to reference zones indicative of a specific removal process. The reference zones were delineated based on results from published laboratory studies, which investigated the processes in isolation. Accordingly, zones for aerobic biodegradation (Hunkeler et al. 2001a; Vogt et al. 2008), anaerobic biodegradation (Mancini et al. 2008; Herrmann et al. 2009; Bergmann et al. 2011), and for volatilization from water or NAPL (Harrington et al. 1999; Wang and Huang 2003) were established (see Appendix S4 for details). For physical removal, the zones represent the isotope trends for equilibrium partitioning among NAPL, water, and air. Mass-transfer limitations (e.g., due to small-scale diffusion) can offset the isotope values from the lines (Kuder et al. 2009). However, the isotope trends remain distinctly different for each process. Dual carbon and hydrogen isotope plots for benzene and toluene in water samples are shown for ML-2A and ML-2C on Figure 5. Results for benzene in additional monitoring locations (ML-1A, -1B, -1C, and ML-2B) are presented in the Figure S8 in Appendix S6. The indicated uncertainty corresponds to the analytical uncertainty (2σ). At real field sites, unknown variations in the source isotopic composition can add further uncertainty.

For benzene, during the prewinter treatment period, the $\delta^{13}C$ and $\delta^{2}H$ values shifted in the positive direction relative to the baseline signature corresponding to an enrichment of heavy isotopes. For ML-2A, the data point was initially (Day 21) located between the two biodegradation zones and then shifted to the aerobic biodegradation zone at Day 44 and Day 60. However, the isotope ratio did not become successively more enriched as would be expected if dissolved benzene had been progressively degraded. At Day 60, the isotope shift at ML-2A had diminished, approaching the isotope signature of the released benzene. This pattern suggests that additional benzene was dissolving from residual NAPL (with a nonimpacted isotope signature). For ML-2C, the benzene data for Day 44 and Day 60 plotted in the anaerobic biodegradation zone (benzene was not detected at Day 21).

At the end of the winter recess (Day 156), the $\delta^{13}C$ and $\delta^{2}H$ values at both sampling locations plotted in the anaerobic zone as expected since the IAS system was not in operation. For the postwinter treatment period, benzene remained initially in or close to the anaerobic zone (Day 187) at both sampling locations. By Day 214, the $\delta^{13}C$ and $\delta^{2}H$ values shifted to the aerobic zone at ML-2A, while at ML-2C the concentrations dropped below the detection limit. Similar to ML-2A and 2C, a general shift of the $\delta^{13}C$ and $\delta^{2}H$ of benzene in a positive direction suggesting biodegradation was also observed for the four additional monitoring locations (Figure S8 in Appendix S6). Hence, isotope data from all six sampling locations suggest that aerobic and anaerobic biodegradation likely dominated over volatilization for benzene. The predominance of biodegradation is in agreement with the compound-specific mass balance (Table 2), indicating that biodegradation removed 82 ± 20% of the total benzene mass.

Toluene also became enriched in heavy isotopes (Figure 5) similar to benzene. At ML-2A, no change was observed at Day 21 likely related to ongoing dissolution from residual NAPL, as suggested by an increasing concentration, while toluene plotted in the aerobic zone at Day 44 and Day 60. By Day 60, the isotope signature approached the origin again due to ongoing dissolution. For ML-2C, the results obtained at Day 44 and Day 60 indicated aerobic biodegradation as well.

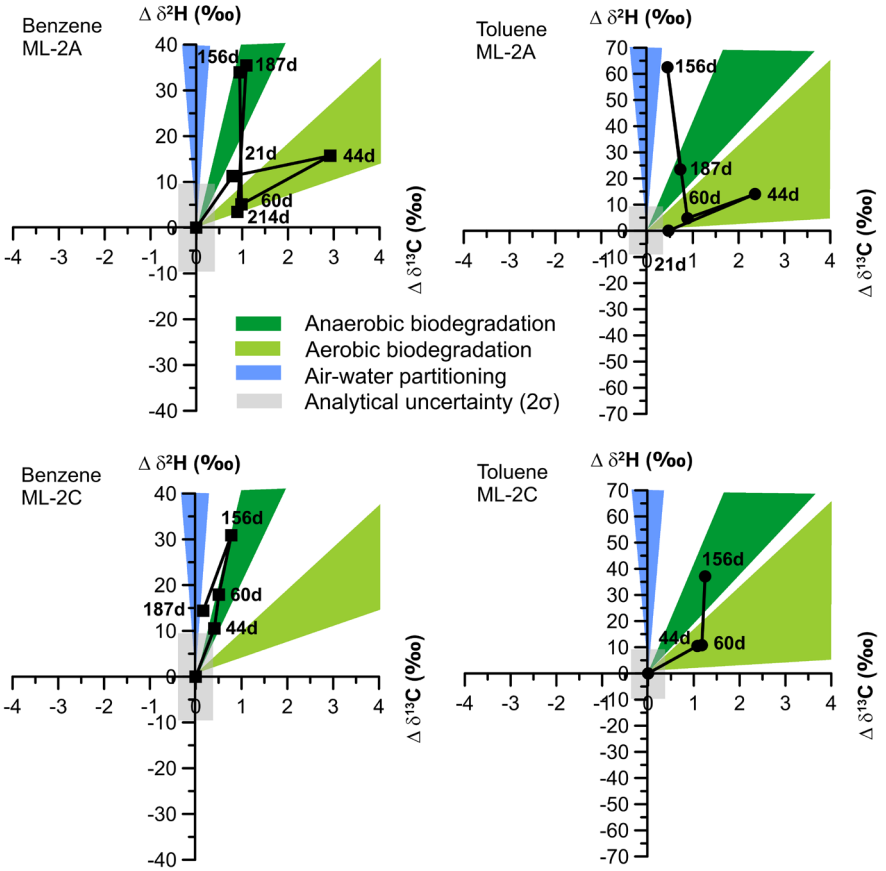

Figure 5. Dual carbon ($\delta^{13}C$) and hydrogen ($\delta^{2}H$) isotope data for benzene and toluene at two groundwater sampling locations (ML-2A and ML-2C) at various times indicated in days (d). The isotope ratios are plotted relative to their initial values. The reference zones are based on the isotope enrichment factors given in Table S4 in Appendix S4.

At the end of the winter recess period (Day 156), the $\delta^{13}C$ and $\delta^{2}H$ values for toluene plotted in the anaerobic zone for ML-2C. For ML-2A, the $\delta^{13}C$ and $\delta^{2}H$ values plotted above the anaerobic zone. Because the sampling was carried out before the IAS system was restarted, a shift of the isotope ratio due to volatilization can be excluded. Therefore, it is more likely that the isotope data at ML-2A reflect anaerobic biodegradation. In the postwinter treatment period (Day 187), the $\delta^{13}C$ and $\delta^{2}H$ values at ML-2A remained in the anaerobic zone while the concentration at ML-2C was below the detection limit.

Overall, CSIA of groundwater samples provide evidence that biodegradation of benzene and toluene was occurring and likely dominated over volatilization, consistent with the compound-specific mass balance (Table 2). The data also suggest that aerobic degradation was established, but in some zones anaerobic degradation still prevailed.

Effluent Gas: Dual element isotope plots for gas phase benzene and isooctane were evaluated to determine if CSIA could discern removal processes based on the system effluent gas even though the effluent gas integrates a signature representative of the entire treatment zone (Figure 6). This evaluation focused on benzene and isooctane because contrasting removal processes are expected for these two compounds as indicated by the compound-specific mass balance (Table 2). Isooctane is very volatile and is also known to be fairly resistant to biodegradation due to its branched molecular structure. For benzene, the $\delta^{13}C$ and $\delta^{2}H$ data shifted in the positive direction consistent with biodegradation and the data from groundwater samples. However, the magnitude of the shift is smaller than observed for some groundwater samples (e.g., ML-2A, Figure 6) likely due to averaging over regions with different degrees of biodegradation. For isooctane, the $\delta^{13}C$ and $\delta^{2}H$ data are located close to the origin while at early time a temporary shift into the air-water partitioning zone is observed (Day 21) and at later time a shift into the air-NAPL equilibration zone is observed. The initial shift could be due to the sparging of the initially dissolved mass, the later shift due to the progressive volatilization of the isooctane directly from NAPL. The contrasting patterns between benzene and isooctane confirm that dual carbon and hydrogen isotope plots can help to discriminate physical removal from biodegradation using samples taken from either groundwater or the effluent gas.

Biomarkers Characteristic for Monoaromatic Hydrocarbons

Results for mRNA assays of genes encoding enzymes that broadly attack monoaromatic hydrocarbons from ML-2 groundwater samples are shown on Figure 7. This well was selected because of the presence of high VOC concentrations and its central location. The mRNA transcripts of *todC* are indicative of aerobic benzene, toluene, or xylene biodegradation, while the *bssA*-SRB mRNA transcripts are

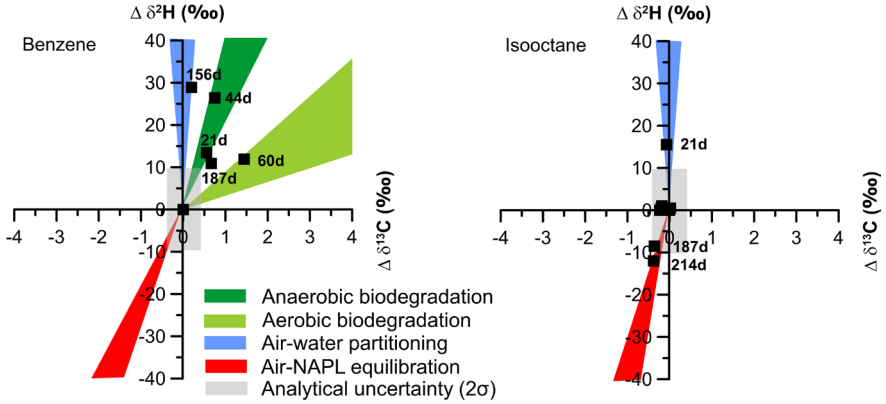

Figure 6. Dual carbon ($\delta^{13}C$) and hydrogen ($\delta^{2}H$) isotope data for benzene and isooctane measured in the effluent gas captured by the vacuum extraction system at various times indicated in days (d). The isotope ratios are plotted relative to their initial values. The reference zones are based on the isotope enrichment factors given in Table S4 in Appendix S4.

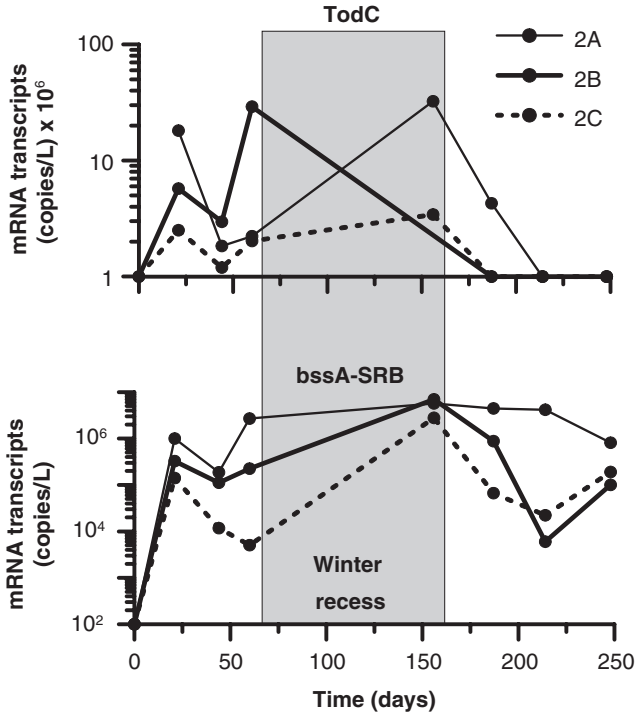

Figure 7. mRNA transcript abundances indicative of aerobic biodegradation of BTX (toluene dioxygenase [*todC*] mRNA) and sulfate-reducing biodegradation of TX (benzyl-succinate synthase of sulfate reducing bacteria [*bssA-SRB*] mRNA). Data are from three monitoring levels (A, B, and C) in ML-2, gathered over 250 days. The IAS system was not operational from Day 60 to Day 156 (winter recess). Detection limits for *todC* and *bssA-SRB* are 8×10^4 and 10^4 copies/L, respectively. The abundance of *abcA* transcript was below detection limit (10^2 copies/L).

characteristic of toluene or xylene biodegradation by sulfate reducing bacteria under anoxic condition. Although absolute numbers of transcript copies measured are reported on Figure 7, interpretation of data from measurements of biomarkers is essentially qualitative. The presence of a given biomarker indicates if the physiological process of biodegradation was in progress at the time the sample was collected. Changes in the quantitative abundance of these biomarkers are an indication of concomitant changes in the contribution of the organisms that carry out the respective process to the total extent of bioremediation of the hydrocarbons. The chosen biomarkers are specific to aerobic or anaerobic biodegradation; thus, they shed light upon both the fate of the compound and the prevailing redox conditions. Absence of a biomarker does not indicate that the biomarker-specific biodegradation process was absent from the sampled location; instead, negative results may indicate that the biomarker was below the analytical detection limit.

Before the source injection, *todC* and *bssA*-SRB mRNA transcript levels were below the detection limit. During the prewinter treatment period (Days 21, 44, and 60), *todC* and *bssA*-SRB mRNA transcripts were detected at all three depths (Figure 7). The concentration of *todC* at Level A increased early in the treatment (Day 21). The transcript was detected throughout the prewinter period at varying concentrations (Days 44 and 60). Similarly, the *bssA*-SRB concentrations increased early in the treatment (Day 21). Following the initial increase, *bssA*-SRB concentrations remained stable at Levels A and B, whereas a decrease was observed at Level C. Detection of both *todC* and *bssA*-SRB mRNA transcripts at Day 21 demonstrates a rapid microbial adaptation to BTX compounds newly introduced into this environment, thus confirming early biodegradation activity upon system startup. Furthermore, detection of both transcripts is consistent with the presence of DO and SO_4^{2-} (Figure 3) that are required to sustain these microbial processes. The co-existence of aerobic and anaerobic biodegradation in the experimental cell as suggested by the biomarkers is consistent with the CSIA data. During the initial part of the prewinter treatment period, BTX concentrations were observed to increase (Figure 2). This increase precludes detection of biodegradation based on contaminant loss, yet biomarkers show evidence for in situ microbial metabolism. Clearly, the biomarker approach offers valuable insights into site-specific processes. In addition, detection of *todC* transcripts demonstrate that aerobic metabolism was active within the cell, consistent with DO concentrations below theoretical saturation (Figure 3)

and a strong depletion of O_2 during periods without sparging in the initial phase of the experiment (Figure S7 in Appendix S6).

During the winter recess, concentrations of *bssA*-SRB transcripts increased considerably (up to 2 orders of magnitude) at all sampling levels (Figure 7) simultaneously with a decrease in SO_4^{2-} (Day 156, Figure 3). Furthermore, concentrations of *todC* mRNA transcripts increased (Level A) or remained stable (Level C), indicating that both types of biodegradation conditions (aerobic and anaerobic) were ongoing during the 3-month winter recess.

During the post-winter treatment period (between Days 156 and 248, Figure 7), *todC* transcripts decreased until no longer detected at Day 187 (Level B and C) or Day 214 (Level A). The content of *bssA*-SRB transcripts also decreased (by approximately one order or magnitude), but were still detected at Day 248. Similar to the pre-winter treatment period, the presence of both types of mRNA transcripts indicate the co-existence of aerobic and anaerobic biodegradation at Level A. The decline in both types of mRNA transcripts was likely due to insufficient BTX mass to sustain the microbial population coding for *todC* and *bssA*-SRB mRNA transcripts. The lower abundance of mRNA transcripts is in agreement with the decreased CO_2 concentration in the effluent gas.

Compound-Specific Biomarkers and Diagnostic Tool Integration

Compound-specific biomarkers (metabolites and mRNA) for aerobic and anaerobic biodegradation of benzene and toluene are presented for ML-2A (Figure 8). Data for additional sampling locations are provided in the Figure S9 of Appendix S6 for ML-3C and Figure S10 for ML-2B of Appendix S6. To compare the response of the different diagnostic tools, CSIA for benzene and toluene, and DO concentrations are also shown in Figure 8. To plot the dual element isotope data as a function of time, consistent with the other data, angular coordinates were attributed to data points on the dual element isotope plots according to a polar coordinate system. Angular coordinates were defined in counterclockwise direction relative to the *x*-axis of the dual element isotope plot. The size of the symbols is proportional to the radial distance from the origin. The transformation into angular coordinates makes it possible to illustrate shifts in position of data points on a dual element isotope plot as function of time. The angular coordinate of

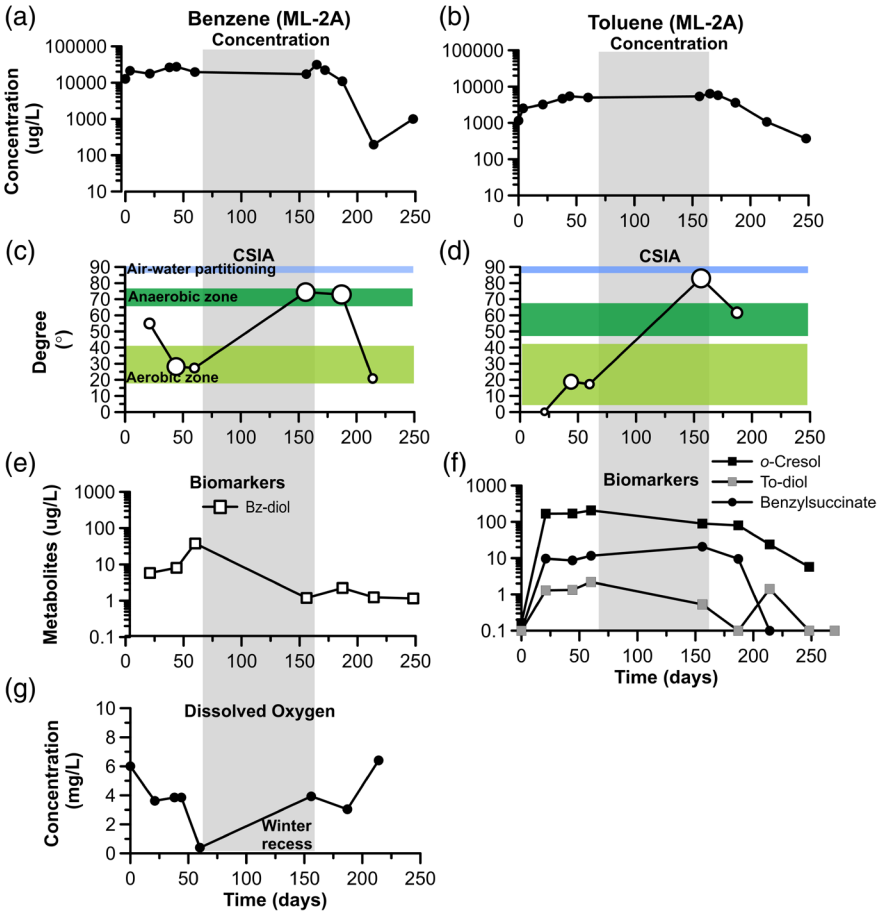

Figure 8. Concentration and diagnostic tool data at ML-2A: concentration of (a) benzene and (b) toluene; CSIA data expressed in angular coordinates of the dual element isotope plot ($\delta^{13}C$ and $\delta^{2}H$) for (c) benzene and (d) toluene (symbol size is proportional to the distance of the data point from the origin); (e) concentration metabolite benzene *cis*-dihydrodiol (Bz-diol) indicative of aerobic benzene degradation; (f) concentration of metabolites toluene *cis*-dihydrodiol (To-diol) and o-cresol indicative of aerobic toluene degradation and benzylsuccinate indicative of anaerobic toluene degradation; (g) concentration of dissolved oxygen. Detection limit for metabolites is 0.1 ug/L.

data points as a function of time was superimposed on the angular coordinate ranges for the reference zones to identify temporal shifts in the mass removal processes (Figure 8).

For benzene, the metabolite benzene-cis-dihydrodiol (Bz-diol) (benzene-specific metabolite strictly produced during aerobic biodegradation) and *abcA* mRNA gene code (benzene-specific mRNA transcript strictly produced during anaerobic biodegradation) were used as parameters indicative of aerobic and anaerobic biodegradation activity, respectively. During the prewinter treatment period, Bz-diol gradually increased and reached its peak at Day 60. During the same period, no *abcA* mRNA transcript was observed (data not shown). Similar patterns were observed for ML-2B (Figure S10 in Appendix S6) and ML-2C (Figure S9 in Appendix S6). The increasing presence of Bz-diol from Day 21 to Day 60 demonstrates the rapid acclimation of the microbial population to benzene and is in agreement with the CSIA data also suggesting aerobic biodegradation during this period (Figure 8). Although DO concentrations were low at Day 60, previous studies showed that aerobic benzene biodegradation can still occur with DO concentration as low as 0.05 mg/L (Yerushalmi et al. 2001). Independent of DO concentration changes, CSIA and biomarkers results confirmed that the system sustained aerobic biodegradation.

At the end of the winter recess period (Day 156), the Bz-diol concentration in ML-2A (also at Levels B and C, see Figures S9 and S10 in Appendix S6) was low suggesting decreasing aerobic biodegradation of benzene during the winter recess. The *abcA* gene transcripts remained below detection limit (data not shown). However, this does not exclude anaerobic biodegradation of benzene, as the expression of abcA genes has been, to date, studied only under iron-reducing conditions (Abu Laban et al. 2010). The CSIA data of benzene plotted in the anaerobic biodegradation zone confirming a transition from aerobic to anaerobic biodegradation. Unexpectedly, at the end of winter recess, DO concentrations increased possibly due to arrival of some oxygenated water related to snowmelt (Figure 8). However, at the deeper locations (ML-2C, see Figure S9 Appendix S6), the DO concentration decreased as expected.

During the postwinter treatment period, Bz-diol concentration in ML-2A remained low until the end of the experiment despite the high benzene concentration observed at Day 187 suggesting that aerobic conditions did not recover immediately after restarting the IAS system. Consistent with this, the isotope values remained in the anaerobic biodegradation zone (Figure 5, Day 187). At later times, low concentrations of metabolites may be related to low benzene concentrations.

For toluene, toluene-cis-dihydrodiol (To-diol), and *o*-cresol (toluene-specific metabolites strictly produced during aerobic biodegradation) were used as an indicator for aerobic biodegradation. Anaerobic biodegradation was evaluated based on benzylsuccinate (toluene-specific metabolite strictly produced during anaerobic biodegradation). All three metabolites were detected during the prewinter treatment period, and concentrations remained stable until Day 60 at Level A (Figure 8) and Levels B and C (see Figures S9 and S10 Appendix S6). CSIA results indicated that aerobic biodegradation conditions dominated during the prewinter treatment period, but the presence of the two types of metabolites indicates that geochemical spatial heterogeneity allowed anaerobic biodegradation to occur in some micro-environment locations. In addition, biomarker results highlight the complementarity of the tools. At Day 21, toluene dissolution from the NAPL impeded CSIA assessment, but metabolites (Figure 8) provided evidence of aerobic biodegradation.

At the end of the winter recess (Day 156), the concentration of aerobic metabolites was lower and the concentration of anaerobic metabolite for benzylsuccinate was higher than at the beginning (Day 60). With dual element isotope data located in the anaerobic biodegradation zone, all diagnostic tools consistently indicated that anaerobic biodegradation of toluene prevailed during this period.

During the postwinter treatment period, aerobic biodegradation of toluene, similar to benzene, did not reestablish immediately after the IAS system restarted. The concentration of aerobic metabolites did not increase, except for the transient increase of To-diol at Day 214 (Figure 8). In parallel, the key anaerobic metabolite (benzylsuccinate) gradually decreased to nondetect levels, but the CSIA data suggested that anaerobic metabolism was predominant in the cell on Day 187. The decrease in both types of metabolites was likely due to the low toluene concentration, relative to the prewinter operational period similar to the trend previously discussed for benzene.

Summary and Conclusions

Diagnostic tools with the potential to assess compound-specific mass removal processes were tested during an IAS pilot-scale study. For this IAS study, it was of particular interest to know if these tools could be used to document shifts from anaerobic to aerobic biodegradation, and to demonstrate that biodegradation occurs in addition to physical (volatilization) removal. The controlled experimental conditions made it possible to compare findings using diagnostic tools with approximate compound-specific mass balances. Furthermore, the occurrence of a winter recess period created additional transience in redox conditions to examine the sensitivity of the diagnostic tools.

The results demonstrated that CSIA and biomarkers are useful for assessing processes that occur during IAS. Both CSIA and biomarkers provided evidence for biodegradation during air sparging and made it possible to document changes from aerobic to anaerobic biodegradation. CSIA data were used to evaluate the intensity and contributions of biodegradation over time as a function of system operation. In the presence of NAPL, CSIA can be considered a transient indicator of biodegradation, analogous to metabolite and mRNA biomarkers that are short-lived and disappear once the responsible process ceases. Ongoing dissolution of target compounds from the NAPL can return the isotope signature to its origin (i.e., baseline value) as observed for some sampling events in this study. While this resetting effect potentially masks isotope fractionation temporally, it has the advantage that subsequent shifts start again from the origin and can thus more easily be related to known reference points. In contrast, interpretation would be more challenging if the isotope shifts associated with different

processes gradually evolve without resetting. Due to this resetting effect in the presence of NAPL, CSIA cannot be applied to quantify biodegradation using, for example, the Rayleigh equation. Rather, isotope data can be used to evaluate if the intensity of biodegradation or another process increases over time or as a function of system operation.

Similar to CSIA, biomarkers cannot provide quantitative information about in situ rates because the relationships between rates of degradation and the abundances of both metabolites and mRNA transcripts are complex. However, biomarkers can be valuable for evaluating the occurrence of biodegradation in NAPL source zones, as they are not affected by NAPL dissolution in contrast to CSIA.

While CSIA and biomarkers share some features, there are also differences. Only CSIA can potentially indicate the relative contribution of biodegradation vs. physical removal as biomarkers do not reflect physical removal processes. However, due to the generally smaller isotope fractionation factors for physical removal processes, their effect only becomes apparent after a large fraction of contaminant mass has been removed. As isotope ratios show a low sensitivity to physical processes in the early phase of SVE, the onset of biodegradation can be identified more easily. Indeed, the comparison of CSIA data for benzene and isooctane with the compound-specific mass balances confirmed that contrasting CSIA patterns can be used to distinguish microbiological vs. physical removal. The diagnostic tools used in this study are also complementary to some of the conventional data collected. While CO_2 mass balances make it possible to quantify the overall rate of biodegradation, CSIA and biomarkers have the advantage of being compound-specific, hence providing the possibility to document the fate of contaminants of concern. In this study, where volatilization contributed to 70% of the overall VOC mass removal, CSIA data confirmed that benzene and toluene were predominantly removed by aerobic and anaerobic biodegradation.

The application of the diagnostic tools explored in this work is likely beneficial during different phases of IAS implementation. For pilot tests, these tools can help to confirm the effectiveness of an IAS system and thus support full-scale design. During full-scale efforts, they can be used to track the dominant mass removal process with an objective to optimize the IAS system operation to maximize treatment, and to identify when the IAS system is no longer able to sustain the intended removal processes. As demonstrated in this study, the diagnostic tools greatly enhanced the possibility to discriminate among mass removal processes on a compound-specific basis, which was particularly valuable when specific compounds are of interest (e.g., benzene). Since CSIA and biomarkers can be used in conjunction with the conventional data collected to evaluate the operation of an IAS system, they provide additional and highly insightful lines of evidence that ultimately strengthen treatment strategies for the management of contaminated sites.

Acknowledgments

We are grateful to laboratory personnel (Bibianne Schlunegger, University of Neuchatel; and Marianne Van der Griendt, Shirley Chatten, Richard Elgood, University of Waterloo) and field personnel (Bob Ingleton and Paul Johnson, University of Waterloo) who contributed to various elements of this research effort. We also thank Kammy Sra (from Chevron) and the two peer-reviewers for their valuable comments on this manuscript. Financial support for this study was provided by Chevron Energy Technology Company.

Supporting Information

The following supporting information is available for this article:

Appendix S1. Analytical methods

Appendix S2. Mass balance calculation

Appendix S3. UVOST assessment and soil core sampling

Appendix S4. Dual element isotope assessment

Appendix S5. Final VOC concentrations

Appendix S6. Supplemental concentration, isotope and biomarker data

Figure S1. Calibration curves (period 1,2,3,4 and 5, see Table S-2) to convert PID readings to total VOC concentration (TVOC ug/L) based on VOC laboratory analysis of effluent gas samples.

Figure S2. CO_2 concentrations continuously measured in the effluent gas using an infrared monitor during the treatment. The gap between day 60 and 156 represents the winter period during which the treatment was stopped.

Figure S3. Comparison of field and laboratory CO_2 analysis.

Figure S4. NAPL distribution in the aquifer as monitored by UVOST before (three left panels) and after (three right panels) the treatment. The orange color between 0 and 1 m (2 to 3 feet) indicates noise/background signals in the unsaturated zone. The yellow, green and light blue colors indicate residual/free NAPL phase.

Figure S5. Plan view of the experimental cell with locations of the three UVOST profiles (A, B and C). Soil sampling was performed at location B.

Figure S6. Change in $\delta^{13}C$ and $\delta^{2}H$ composition of isooctane caused by air-water partitioning (A and B) and by NAPL-vapor equilibration (C and D).

Figure S7. Changes in the proportion of O_2 and CO_2 in the extracted gas during 3 sampling events before (left side) and after (right side) winter recess.

Figure S8. Concentration and isotope ($\delta^{13}C$ and $\delta^{2}H$) changes for benzene measured in four additional groundwater sampling points.

Figure S9. Patterns in the concentrations of benzene and toluene (top), corresponding polar coordinate trajectories of CSIA dual isotope ($\delta^{13}C$ and $\delta^{2}H$) plots, concentrations of compound-specific biomarkers, and dissolved oxygen. Detection limits for *abcA* transcript and metabolites are respectively 10^2 copies/L and 0.1 ug/L.

Figure S10. Compound-specific metabolites and mRNA transcripts measured for benzene (A) and toluene (B) in ML-2B at various sampling periods during the sparging treatment. Abbreviations: Tol, toluene; Bz, benzene. Detection limits for *abcA* transcript and metabolites are respectively 10^2 copies/L and 0.1 ug/L.

Table S1. PCR primers used in this study.

Table S2. Intervals for mass balance calculations according to changing VOC proportions and air flow rates.

Table S3. Concentrations of metabolites specific for aerobic toluene degradation during the sparging treatment. Some metabolites are characteristic for ring-attack (toluene cis-dihydrodiols, o-cresol and p-cresol) other for methyl-group attack (benzyl alcohol)

Table S4. Air-water partitioning and NAPL-vapor equilibration isotope enrichment factors (C and H) for benzene, toluene and isooctane.

Table S5. Final concentration measurement of VOC dissolved in groundwater (ug/L).

Table S6. Final concentration measurement of VOC in soil (day 380) (mg/kg).

References

Abu Laban, N., D. Selesi, T. Rattei, P. Tischler, and R.U. Meckenstock. 2010. Identification of enzymes involved in anaerobic benzene degradation by a strictly anaerobic iron-reducing enrichment culture. *Environmental Microbiology* 12: 2783–2396.

Aelion, C.M., and B.C. Kirtland. 2000. Physical versus biological hydrocarbon removal during air sparging and soil vapor extraction. *Environmental Science & Technology* 34, no. 15: 3167–3173.

Aelion, C.M., P. Hoehener, D. Hunkeler, and R. Aravena. 2010. *Environmental Isotopes in Biodegradation and Bioremediation*, Vol. 450. Boca Raton, Florida: CRC Press, Taylor and Francis Group.

Bass, D.H., N.A. Hastings, and R.A. Brown. 2000. Performance of air sparging systems: A review of case studies. *Journal of Hazardous Materials* 72, no. 2–3: 101–119.

Beller, H.R., W.H. Ding, and M. Reinhard. 1995. By-product of anaerobic alkylbenzene metabolism useful as indicators of in-situ bioremediation. *Environmental Science & Technology* 29, no. 11: 2864–2870.

Beller, H.R., S.R. Kane, T.C. Legler, J.R. McKelvie, B. Sherwood Lollar, F. Pearson, L. Balser, and D.M. Mackay. 2008. Comparative assessments of benzene, toluene, and xylene natural attenuation by quantitative polymerase chain reaction analysis of a catabolic gene, signature metabolites, and compound-specific isotope analysis. *Environmental Science & Technology* 42, no. 16: 6065–6072.

Bergmann, F.D., N.M.F.H. Abu Laban, A.H. Meyer, M. Elsner, and R.U. Meckenstock. 2011. Dual (C, H) isotope fractionation in anaerobic low molecular weight (poly)aromatic hydrocarbon (PAH) degradation: Potential for field studies and mechanistic implications. *Environmental Science & Technology* 45, no. 16: 6947–6953.

Berkey, J.S., T.E. Lachmar, W.J. Doucette, and R. Ryan Dupont. 2003. Tracer studies for evaluation of in situ air sparging and in-well aeration system performance at a gasoline-contaminated site. *Journal of Hazardous Materials* 98, no. 1–3: 127–144.

Bomback, P., H.H. Richnow, M. Kastner, and A. Fisher. 2010. Current approaches for the assessment of in situ biodegradation. *Applied Microbiology and Biotechnology* 86: 839–852.

Bouchard, D., and D. Hunkeler. 2014. Solvent-based dissolution method to sample gas-phase volatile organic compounds for compound-specific isotope analysis. *Journal of Chromatography. A* 1325: 16–22.

Bouchard, D., P.W. McLoughlin, D. Hunkeler, and R.J. Pirkle. 2015. ^{13}C and $\delta^{37}Cl$ on gas-phase TCE for source identification investigation – Innovative solvent-based sampling method. Paper presented at Environmental Forensics*:* Proceedings of the 2014 INEF Conference. Cambridge, UK.

Bruce, C.L., I.L. Amerson, R.L. Johnson, and P.C. Johnson. 2001. Use of an SF 6-based diagnostic tool for assessing air distributions and oxygen transfer rates during IAS operation. *Bioremediation Journal* 5, no. 4: 337–347.

Buscheck, T., T. Kuder, P. Philp, R. Kolhatkar, and L. Klinchuch. 2009. Two-dimensional compound-specific isotope analysis to assess remediation system effectiveness. Paper presented at In Situ and on-Site Bioremediation – Tenth International In Situ and On-Site Bioremediation Symposium. Baltimore, Maryland: Battelle Memorial Institute.

Busi da Silva, M.L., and H.X. Corseuil. 2012. Groundwater microbial analysis to assess enhanced BTEX biodegradation by nitrate injection at a gasohol-contaminated site. *International Biodeterioration & Biodegradation* 67: 21–27.

Cébron, A., M.P. Norini, T. Beguiristain, and C. Leyval. 2008. Real-time PCR quantification of PAH-ring hydroxylating dioxygenase (PAH-RHDα) genes from Gram positive and Gram negative bacteria in soil and sediment samples. *Journal of Microbiological Methods* 73: 148–159.

Diaz, E.J., I. Jiménez, and J. Nogales. 2013. Aerobic degradation of aromatic compounds. *Current Opinion in Biotechnology* 24: 431–442.

Elsner, M., L. Zwank, D. Hunkeler, and R.P. Schwarzenbach. 2005. A new concept linking observable stable isotope fractionation to transformation pathways of organic pollutants. *Environmental Science & Technology* 39, no. 18: 6896–6916.

Fuchs, G., M. Boll, and H. J. 2011. Microbial degradation of aromatic compounds — From one strategy to four. *Nature Reviews Microbiology* 9: 803–816.

Griebler, C., M. Safinowski, A. Vieth, H.H. Richnow, and R.U. Meckenstock. 2004. Combined application of stable carbon isotope analysis and specific metabolites determination for assessing in situ degradation of aromatic hydrocarbons in a tar oil-contaminated aquifer. *Environmental Science & Technology* 38, no. 2: 617–631.

Hall, B.L., T.E. Lachmar, and R.R. Dupont. 2000. Field monitoring and performance evaluation of an in situ air sparging system at a gasoline-contaminated site. *Journal of Hazardous Materials* B74: 165–186.

Harrington, R.R., S.R. Poulson, J.I. Drever, P.J.S. Colberg, and E.F. Kelly. 1999. Carbon isotope systematics of monoaromatic hydrocarbons: Vaporization and adsorption experiments. *Organic Geochemistry* 30, no. 8A: 765–775.

Hendrickx, B.H., H. Junca, J. Vosahlova, A. Lindner, I. Ruegg, M. Bucheli-Witschel, F. Faber, T. Egli, M. Mau, D.H. Pieper, E.M. Top, W. Dejonghe, L. Bastiaens, and D. Springael. 2006. Alternative primer sets for PCR detection of genotypes involved in bacterial aerobic BTEX degradation: Distribution of the genes in BTEX degrading isolates and in subsurface soils of a BTEX contaminated industrial site. *Journal of Microbiological Methods* 64: 250–265.

Herrmann, S., C. Vogt, A. Fischer, A. Kuppardt, and H.-H. Richnow. 2009. Characterization of anaerobic xylene biodegradation by two-dimensional isotope fractionation analysis. *Environmental Microbiology Reports* 1, no. 6: 535–544.

Hunkeler, D., N. Anderson, R. Aravena, S.M. Bernasconi, and B.J. Butler. 2001a. Hydrogen and carbon isotope fractionation during aerobic biodegradation of benzene. *Environmental Science & Technology* 35, no. 17: 3462–3467.

Hunkeler, D., B.J. Butler, R. Aravena, and J. Barker. 2001b. Monitoring biodegradation of methyl tert-butyl ether (MTBE) using compound-specific carbon isotope analysis. *Environmental Science & Technology* 35: 676–681.

Jeon, C.O., and E.L. Madsen. 2013. In situ microbial metabolism of aromatic-hydrocarbon environmental pollutants. *Current Opinion in Biotechnology* 24: 474–481.

Johnson, P.C., R.L. Johnson, C. Neaville, E.E. Hansen, S.M. Stearns, and I.J. Dortch. 1997. An assessment of conventional in situ air sparging pilot tests. *Ground Water* 35, no. 5: 765–774.

Johnson, R.L., P.C. Johnson, T.L. Johnson, and A. Leeson. 2001a. Helium tracer tests for assessing contaminant vapor recovery and air distribution during in situ air sparging. *Bioremediation Journal* 5, no. 4: 321–336.

Johnson, R.L., P.C. Johnson, T.L. Johnson, N.R. Thomson, and A. Leeson. 2001b. Diagnosis of in situ air sparging performance using transient groundwater pressure changes during startup and shutdown. *Bioremediation Journal* 5, no. 4: 299–320.

Johnston, C.D., J.L. Rayner, B.M. Patterson, and G.B. Davis. 1998. Volatilisation and biodegradation during air sparging of dissolved contaminated groundwater. *Journal of Contaminant Hydrology* 33, no. 3–4: 377–404.

Kao, C.M., C.Y. Chen, S.C. Chen, H.Y. Chien, and Y.L. Chen. 2008. Application of in situ biosparging to remediate a petroleum-hydrocarbon spill site: Field and microbial evaluation. *Chemosphere* 70: 1492–1499.

Krembs, F.J., R.L. Siegrist, M.L. Crimi, R.F. Furrer, and B.G. Petri. 2010. ISCO for groundwater remediation: Analysis of field applications and performance. *Groundwater Monitoring and Remediation* 30, no. 4: 42–53.

Kuder, T., P. Philp, and J. Allen. 2009. Effects of volatilization on carbon and hydrogen isotope ratios of MTBE. *Environmental Science & Technology* 43, no. 6: 1763–1768.

Landmeyer, J.E., D.A. Vroblesky, and F.H. Chapelle. 1996. Stable carbon evidence of biodegradation zonation in a shallow jet-fuel contaminated aquifer. *Environmental Science & Technology* 30: 1120–1128.

Liu, J.B., T. Amemiya, Q. Chang, X. Xu, and K. Itoh. 2011. Real-time reverse transcription PCR analysis of trichloroethylene-regulated toluene dioxygenase expression in Pseudomonas putida F1. *Journal of Environmental Science and Health, Part B: Pesticides, Food Contaminants, and Agricultural Wastes* 46, no 4: 294–300.

Mackay, D.M., D.L. Freyberg, P.V. Roberts, and J.A. Cherry. 1986. A natural gradient experiment on solute transport in a sand aquifer. 1. Approach and overview of plume movement. *Water Resources Research* 22, no. 13: 2017–2029.

Madsen, E.L. 1991. Determining in situ biodegradation: Facts and challenges. *Environmental Science & Technology* 25: 1662–1673.

Madsen, E.L. 2000. Nucleic-acid characterization of the identity and activity of subsurface microorganisms. *Hydrogeology Journal* 8, no. 1: 112–125.

Mancini, S.A., C.E. Devine, M. Elsner, M.E. Nandi, A.C. Ulrich, E.A. Edwards, and B.S. Lollar. 2008. Isotopic evidence suggests different initial reaction mechanisms for anaerobic benzene biodegradation. *Environmental Science & Technology* 42, no. 22: 8290–8296.

Martienssen, M., H. Fabritius, S. Kukla, G.U. Balcke, E. Hasselwander, and M. Schirmer. 2006. Determination of naturally occurring MTBE biodegradation by analysing metabolites and biodegradation by-products. *Journal of Contaminant Hydrology* 87, no. 1–2: 37–53.

Martus, P., and W. Schaal. 2010. Metabolite analysis as direct proof of biodegradation: Experience from monitored natural attenuation (MNA) projects. *Environmental Forensics* 11, no. 1–2: 94–101.

Morasch, B., D. Hunkeler, J. Zopfi, B. Temime, and P. Hoehener. 2011. Intrinsic biodegradation potential of aromatic hydrocarbons in an alluvial aquifer – Potentials and limits of signature metabolite analysis and two stable isotope-based techniques. *Water Research* 45, no. 15: 4459–4469.

NAVFAC. 2005. Cost and performance report multi-site in situ air sparging. Technical Report No. TR-2260-ENV. NAVFAC.

Nebe, J., B.R. Baldwin, R.L. Kassab, L. Nies, and C.H. Nakatsu. 2009. Quantification of aromatic oxygenase genes to evaluate enhanced bioremediation by oxygen releasing materials at a gasoline-contaminated site. *Environmental Science & Technology* 43, no. 6: 2029–2034.

Nelson, L., J. Barker, T. Li, N. Thomson, M. Ioannidis, and J. Chatzis. 2009. A field trial to assess the performance of CO_2-supersaturated water injection for residual volatile LNAPL recovery. *Journal of Contaminant Hydrology* 109: 82–90.

RaeSystems. 2016. A guideline for PID instrument response. Technical Note No. TN-106. RaeSystems.

Rahbeh, M.E., and R.H. Mohtar. 2007. Application of multiphase transport models to field remediation by air sparging and soil vapor extraction. *Journal of Hazardous Materials* 143: 156–170.

Rogers, S.W., and S.K. Ong. 2000. Influence of porous media, airflow rate, and air channel spacing on benzene NAPL removal during air sparging. *Environmental Science & Technology* 34: 764–770.

Slater, G.F., H.S. Dempster, B.S. Lollar, and J. Ahad. 1999. Headspace analysis: A new application for isotopic characterization of dissolved organic contaminants. *Environmental Science & Technology* 33, no. 1: 190–194.

Sudicky, E.A. 1986. A natural gradient experiment on solute transport in a sand aquifer: Spatial variability of hydraulic conductivity and its role in the dispersion process. *Water Resources Research* 22, no. 13: 2069–2082.

Suthersan, S.S., and F.C. Payne. 2004*In Situ Remediation Engineering*. CRC Press, Boca Raton, USA.

Tomlinson, D.W., N.R. Thomson, R.L. Johnson, and J.D. Redman. 2003. Air distribution in the Borden aquifer during in situ air sparging. *Journal of Contaminant Hydrology* 67: 113–132.

Vogt, C., E. Cyrus, I. Herklotz, D. Schlosser, A. Bahr, S. Herrmann, H.-H. Richnow, and A. Fischer. 2008. Evaluation of toluene degradation pathways by two-dimensional stable isotope fractionation. *Environmental Science & Technology* 42, no. 21: 7793–7800.

Waduge, W.P.A., K. Soga, and J. Kawabata. 2004. Effect of NAPL entrapment conditions on air sparging remediation efficiency. *Journal of Hazardous Materials* 110: 173–183.

Wang, Y., and Y. Huang. 2003. Hydrogen isotopic fractionation of petroleum hydrocarbons during vaporization: Implications for assessing artificial and natural remediation of petroleum contamination. *Applied Geochemistry* 18, no. 10: 1641–1651.

Weissmann, G.S., A. Pickel, K.C. McNamara, J.D. Frechette, I. Kalinovich, R.M. Allen-King, and I. Jankovic. 2015. Characterization and quantification of aquifer heterogeneity using outcrop analogs at the Canadian Forces Base Borden, Ontario, Canada. *Geological Society of America Bulletin*: 127, no. 7-8: 1021–1035.

Whited, G.M., and D.T. Gibson. 1991. Toluene-4-monooxygenase, a three-component enzyme system that catalyzes the oxidation of toluene to p-cresol in Pseudomonas mendocina KR1. *Journal of Bacteriology* 173: 3010–3016.

Whiticar, M.J. 1999. Carbon and hydrogen isotope systematics of bacterial formation and oxidation of methane. *Chemical Geology* 161: 291–314.

Wilson, M.S., and E.L. Madsen. 1996. Field extraction of a unique intermediary metabolite indicative of real time in situ pollutant biodegradation. *Environmental Science & Technology* 30: 2099–2103.

Yaws, C.L. 1999. *Chemical Properties Handbook*. New York: McGraw-Hill Education, New York, USA.

Yerushalmi, L., J.F. Lascourreges, C. Rhofir, and S.R. Guiot. 2001. Detection of intermediate metabolites of benzene biodegradation under microaerophilic conditions. *Biodegradation* 12, no. 6: 379–391.

Zwank, L., M. Berg, M. Elsner, T.C. Schmidt, R.P. Schwarzenbach, and S.B. Haderlein. 2005. New evaluation scheme for two-dimensional isotope analysis to decipher biodegradation processes: Application to groundwater contamination by MTBE. *Environmental Science & Technology* 39, no. 4: 1018–1029.

Biographical Sketches

Daniel Bouchard, *Ph.D., is Research Fellow at the Centre for Hydrogeology and Geothermics, University of Neuchatel, Rue Emile Argand 11, CH-2000 Neuchâtel, Switzerland and R&D Expertise Manager at Sanexen Services Environnementaux Inc., 9935 Avenue de châteauneuf, Bureau 200, Brossard, Québec J4Z 3V4, Canada.*

Massimo Marchesi*, Ph.D., is Postdoctoral Fellow in the Department of Civil and Environmental Engineering, University of Waterloo, Waterloo N2L 3G1, Ontario, Canada. Now a Research Fellow at Politecnico di Milano, Department of Civil and Environmental Engineering, 32 Piazza L. Da Vinci, Milano, MI 20133, Italy.*

Eugene L. Madsen, *Ph.D., Deceased,* ***is*** *Professor in the Department of Microbiology, Cornell University, 125 Wing Dr., Ithaca, NY 14853.*

Christopher M. DeRito, *M.S.,* ***is*** *Research Support Specialist in the Department of Microbiology, Cornell University, 125 Wing Drive, Ithaca, NY 14853.*

Neil R. Thomson*, Ph.D., P.Eng., is Professor in the Department of Civil and Environmental Engineering, University of Waterloo, 200 University Ave. West, Waterloo, Ontario N2L 3G1, Canada.*

Ramon Aravena*, Ph.D., is Emeritus and Adjunct Professor in the Department of Earth and Environmental Science, University of Waterloo, 200 University Avenue West, Waterloo, Ontario N2L 3G1, Canada.*

Jim F. Barker*, Ph.D., is Emeritus Professor in the Department of Earth and Environmental Science, University of Waterloo, 200 University Avenue West, Waterloo, Ontario N2L3G1, Canada.*

Tim Buscheck*, M.S., is Chevron Fellow and Senior Consulting Hydrogeologist in the Health, Environment, and Safety Department, Chevron Energy Technology Company, 6001 Bollinger Canyon Rd., San Ramon, CA 94583.*

Ravi Kolhatkar*, Ph.D., MBA, is Senior Staff Hydrogeologist in the Health, Environment, and Safety Department, Chevron Energy Technology Company, 1400 Smith St., Houston, TX 77002.*

Eric J. Daniels*, Ph.D., is Consulting Hydrogeologist in the Health, Environment, and Safety Department, Chevron Energy Technology Company, 6001 Bollinger Canyon Road, San Ramon, CA 94583.*

Daniel Hunkeler*, Ph.D., corresponding author, is Professor and Director of the Centre for Hydrogeology and Geothermics (CHYN), University of Neuchâtel, CH-2000 Neuchâtel, Switzerland and Adjunct Professor, Department of Earth and Environmental Sciences, University of Waterloo, Waterloo N2L 3G1, Ontario, Canada; daniel.hunkeler@unine.ch*